

X-RAYING EXTENDED EMISSION AND RAPID DECAY OF SHORT GAMMA-RAY BURSTS

YASUAKI KAGAWA¹, DAISUKE YONETOKU¹, TATSUYA SAWANO¹, ASUKA TOYANAGO¹, TAKASHI NAKAMURA², KEITARO TAKAHASHI³, KAZUMI KASHIYAMA⁴, AND KUNIHITO IOKA^{5,6}

Received 2015.05.30; Accepted

ABSTRACT

Extended emission is a mystery in short gamma-ray bursts (SGRBs). By making time resolved spectral analyses of brightest nine events observed by *Swift* XRT, we obviously classify the early X-ray emission of SGRBs into two types. One is the extended emission with exponentially rapid decay, which shows significant spectral softening during hundreds seconds since the SGRB trigger and is also detected by *Swift*-BAT. The other is a dim afterglow only showing power-law decay over 10⁴ s. The correlations between the temporal decay and spectral indices of the extended emissions are inconsistent with the α - β correlation expected for the high-latitude curvature emission from a uniform jet. The observed too-rapid decay suggests the emission from a photosphere or a patchy surface, and manifests the stopping central engine via such as magnetic reconnection at the black hole.

Subject headings: gamma-ray burst; short gamma-ray burst; gravitational wave

1. INTRODUCTION

Short Gamma-Ray Burst (SGRB) is a sub-category of gamma-ray burst phenomena. The SGRB lightcurve is composed of an intense prompt emission with short time duration less than 2 sec and an extended soft X-ray emission lasting about 100 sec in some cases. The integrated energy of both emissions are almost comparable, which motivates us to make detailed studies of the X-ray properties.

The origin of SGRB is still in debate. A major candidate is a coalescence of compact objects, such as neutron stars and black holes (Paczynski 1986; Eichler et al. 1989). Recently, in the afterglow of GRB 130603B, re-brightening in red or near infrared band, a so-called macronova (or kilonova), was observed, and its physical interpretation is discussed as nuclear decay of neutron-rich r-process (rapid-process) elements synthesized in the ejecta of a neutron star binary coalescence (Tanvir et al. 2013; Berger, Fong & Chornock 2013; Berger 2014). There are also other possibilities that the macronova is energized by the extended activity of the central engine (Kisaka et al. 2015) and/or dust emission (Takami et al. 2014).

In the compact merger scenario, the SGRB prompt emission is powered by a relativistic jet launched from the remnant compact object surrounded by a massive disk. The central engine would be black holes (Fan et al. 2005;

Rosswog 2007; Lee et al. 2009; Barkov & Pozanenko 2011; Nakamura et al. 2014; Kisaka & Ioka 2015), or rapidly-spinning strongly-magnetized neutron stars (millisecond magnetars; Usov 1992; Zhang & Mészáros 2001; Gao & Fan 2006; Metzger et al. 2008; Bucciantini et al. 2012; Gompertz et al. 2013; Zhang 2013), depending on the type of coalescing binaries and the equation of state of neutron star matter (Hotokezaka et al. 2011; Kyutoku et al. 2013, 2015). The origin of the extended emission is rather puzzling; the observed duration is longer than the typical accretion time of the disk. It has been proposed that the longer activity can be powered by fallback accretion of tidally stripped matter (Lee et al. 2009; Kisaka & Ioka 2015) or spindown of magnetars (Metzger et al. 2008).

If the compact merger scenario is the case, we expect to detect strong gravitational waves by the second generation gravitational wave observatories, Advanced-LIGO⁷, Advanced-VIRGO⁸ and KAGRA⁹. To pioneer the gravitational wave astronomy, synchronized observations of electromagnetic counterparts in multi-wavelengths are required. Wide field monitoring in X-ray band is an important method to discover the prompt emission and extended soft X-ray emission of SGRBs accompanying the gravitational wave detection.

This paper is constructed as follows. In the next section, we systematically investigate X-ray properties of bright 9 SGRBs. Especially, we perform the time resolved spectral analyses for the extended soft X-ray emission and X-ray afterglows. We show that strong spectral evolution is a common property of the rapid decay phase that follows the extended emission of SGRBs. Finally, in § 3, we discuss the association between the extended soft X-ray emission and the rapid decay, and their spectral and temporal properties. We find that the decay is more rapid than the simple high-latitude emission and discuss interesting implications. Moreover we discuss a population statistics having bright extended emissions.

kagawa@astro.s.kanazawa-u.ac.jp

yonetoku@astro.s.kanazawa-u.ac.jp

¹ College of Science and Engineering, School of Mathematics and Physics, Kanazawa University, Kakuma, Kanazawa, Ishikawa 920-1192, Japan

² Department of Physics, Kyoto University, Kyoto 606-8502, Japan

³ Faculty of Science, Kumamoto University, Kurokami, Kumamoto, 860-8555, Japan

⁴ Einstein fellow — Department of Astronomy; Department of Physics; Theoretical Astrophysics Center; University of California, Berkeley, Berkeley, CA 94720, USA

⁵ Theory Center, Institute of Particle and Nuclear Studies, KEK, Tsukuba 305-0801, Japan

⁶ Department of Particle and Nuclear Physics, SOKENDAI (the Graduate University for Advanced Studies), Tsukuba 305-0801, Japan

⁷ <http://www.ligo.caltech.edu/>

⁸ <http://www.ego-gw.it/index.aspx/>

⁹ <http://gwcenter.icrr.u-tokyo.ac.jp/en/>

2. OBSERVATIONS & DATA ANALYSES

2.1. Data Selection

We first select 79 SGRBs with the time duration of $T_{90} < 2.0$ sec from *Swift* gamma-ray burst catalog until the end of 2014. Here T_{90} is measured as the duration of the time interval during which 90 % of the total observed counts have been detected. However, considering that several SGRBs show the extended soft X-ray emission lasting ~ 100 sec just after the short prompt emission, the above criterion may be insufficient to select samples of interest. We check the individual lightcurves and pick up events with an initial spike of prompt emission followed by rather gradual time sequence. Then, we additionally include possible 13 SGRB candidates reported in GCN circulars¹⁰.

We use data of X-ray afterglows and/or extended X-ray emission observed by Burst Alert Telescope (BAT) and X-ray telescope (XRT) aboard *Swift* to investigate X-ray properties of SGRBs. For our purpose, we need enough number of X-ray photons to perform time-resolved spectral analyses. Thus, we adopt a selection criterion of $F \geq 10^{-11}$ erg cm⁻²s⁻¹ in 2 – 10 keV band at the XRT observation start time. Hereafter, we treat selected 9 samples, GRB 050724, 051221A, 060313, 070714B, 080503, 090510, 100702A, 120804A, and 130603B.

2.2. Swift-BAT lightcurves

In Figure 1, we show the SGRB lightcurves observed with BAT. In Figure 1, each panel shows two kinds of information, i.e., main panels show the initial spike of prompt emission with 128 msec time resolution in 15 – 150 keV band, and inserted panels show the following hard X-ray emission up to 200 sec since the SGRB trigger time with 8 sec time resolution in 15 – 25 keV band.

We adopted a null-flux constant model for data with 8 sec time bin in a time between 8 – 200 sec since SGRB trigger time (except for the first 8 sec to avoid the contribution from prompt emission). We summarized the fitting results in Table 1. As also clearly seen in Figure 1, the extended X-ray emission is detected in 3 samples of GRB 050724, 070714B, and 080503, with T_{90} duration of 98.7 sec, 65.2 sec and 274.9 sec, respectively.

According to these analyses, the other 6 events are fully consistent with no bright extended X-ray emission after the initial spike in BAT data. We searched the extended X-ray emission with several time durations from 8 sec since the trigger time. However we failed to detect any obvious indication of extended X-ray emission in these 6 events.

2.3. Spectral Analyses of XRT data

At first, we extracted an X-ray signal within the image region of 40×30 rectangular pixels with rotation angle of spacecraft for windowed timing (WT) mode data, and 20 pixels in radius (corresponding to ~ 47 arcsec) for photon counting (PC) mode data. These are recommended region size described in the *Swift* XRT software guide. We extracted a background signal from the image region with no X-ray sources (under the sensitivity of XRT).

¹⁰ GRB 050724, 050911, 051227, 060717, 061006, 070714B, 080123, 080503, 090309, 100213A, 100816A, 130716A, and 130822A

The region size is the rectangular with 30×30 pixels for WT mode, and the circle as large as possible (at least 20 pixels) for PC mode data. The source and background regions do not overlap each other.

After that, we performed time resolved spectral analyses for both WT and PC data of selected 9 SGRBs. To conserve the uniform statistical uncertainty for each spectrum, we divided the entire data into several time bins to keep the same number of photons (about 512 photons for WT mode, and 256 photons for PC mode). Then we obtained at least 4 spectra for each SGRBs.

We adopted two kinds of spectral models, i.e. a power-law and a blackbody function. We include galactic and extra-galactic column densities (“phabs” model) for each time resolved data. The exact formulas are as follows;

$$N(E) = \exp\left(-(N_H^{gal} + N_H^{ext})\sigma(E)\right) \times K \left(\frac{E}{1 \text{ keV}}\right)^{-\Gamma} \quad (1)$$

for the power-law model, and

$$N(E) = \exp(-(N_H^{gal} + N_H^{ext})\sigma(E)) \times \left(\frac{K \times 8.0525 E^2 dE}{(kT)^4 [\exp(E/kT) - 1]}\right) \quad (2)$$

for the blackbody model, respectively. Here, $N(E)$ is in units of photons cm⁻² s⁻¹ keV⁻¹. N_H^{gal} and N_H^{ext} are a galactic and an extra-galactic hydrogen column density, in units of 10^{22} atoms cm⁻², respectively, and $\sigma(E)$ is a photo-electric cross-section (not including Thomson scattering). Γ is a photon index, and kT is a temperature in units of keV. The parameters K in both functions are normalization.

We show representative spectra of GRB 080503 in Figure 2. The left and right panels of Figure 2 show the best fit results with the power-law and blackbody model, respectively. The power-law model can well describe the entire shape of the observed spectrum, while the blackbody model has large discrepancies between data and the model around the low- and high-energy region.

In Figure 3, we show reduced χ^2 distribution as a function of time since GRB 080503 trigger. The reduced χ^2 values of the power-law model (open and filled squares for WT and PC mode) and blackbody model (open and filled circles for WT and PC mode) systematically locate around 1 and 2 throughout the entire epoch, respectively. Therefore we can conclude that the observed spectra can be described by the power-law model, and the blackbody model is not suitable for the X-ray spectra after ~ 100 seconds of SGRBs. In the other 8 events, all spectra can be described by the power-law model well.

2.4. Spectral Softening

We summarized the fitting results of spectral parameters, the energy flux in units of 10^{-12} erg cm⁻²s⁻¹ in 2 – 10 keV band (top panel), photon index Γ (middle panel), and the extra-galactic column density N_H^{ext} (bottom panel) in Figure 4. As shown in the figure, at least for 5 samples (GRB 050724, 060313, 070714B, 080503, and 100702A), the photon indices drastically change as a function of time, especially in the early decay phase while N_H is rather stable.

For example, the brightest case of GRB 050724 shows the spectral evolution from $\Gamma \sim 1.2$ to 3.0 for 300 sec since the SGRB trigger time. GRB 070714B, 080503 and 100702A also show rapid spectral softening during

200 – 500 sec since each SGRB trigger. Only one case of GRB 060313 shows gradual softening over 10^4 sec.

2.5. Decay slopes of lightcurves

In Figure 4, the energy fluxes are estimated by the spectral fitting, although almost all previous works converted the photon flux to the energy flux with averaged spectral parameters. Then we investigated the temporal behaviour with three models, i.e., single power-law (PL), broken power-law (BPL), and exponential (EXP) functions. We summarize the fitting results in Table 2. Because of small flaring activities or some fluctuations of the early X-ray afterglows, the reduced χ^2 values are rather large. However the PL model is acceptable for 5 SGRBs, GRB 051221A, 060313, 070714B, 120804A, and 130603B.

On the other hand, we could significantly improve the fitting results with BPL and/or EXP models compared with PL model for the other 4 SGRBs, GRB 050724, 080503, 090510, and 100702A. Especially for 3 events (GRB 050724, 080503, and 100702A), their temporal indices after the break time are remarkably steep. In the remaining GRB 090510, the BPL model is better than the PL model, but the temporal index is gentle 1.97 ± 0.35 even after the break, which is different from the previous three events. When we adopt EXP model to the X-ray lightcurves of GRB 050724, 080503, and 100702A, the time constant is obtained as 50 – 100 sec (see Table 2). The redshift is measured only for GRB 050724 as $z = 0.258$, and then the intrinsic time constant is 41.5 ± 0.7 sec in this case.

3. DISCUSSION

We systematically studied X-ray properties of SGRBs for the brightest 8 events observed by *Swift*-XRT. We performed time resolved spectral analyses for all events, and measured energy fluxes taking the spectral parameters in each time bin into account. In this section, we discuss the observed X-ray properties of SGRBs, and classify them into two types.

3.1. Connection between Extended X-ray Emission and Rapid Decay

Comparing Figure 1 and Figure 4, three SGRBs with the obvious extended X-ray emission in *Swift*-BAT lightcurves (GRB 050724, 070714B, and 080503) have the strong spectral softening and also show rapid decay for two of them (GRB 050724, 080503). GRB 100702A did not have strong extended emission in the BAT lightcurve while it shows spectral softening. The extended emission of GRB 100702A is most likely under the sensitivity of *Swift*-BAT since the X-ray flux in *Swift*-XRT is dimmer than the other three events in Figure 4. These results are summarized in Table 3.

On the other hand, the remaining 5 events without extended emission in *Swift*-BAT lightcurves (GRB 051221A, 060313, 090510, 120804A, and 130603B) do not show the rapid decay phase, and their X-ray lightcurves are almost fully consistent with single power-law decay in *Swift*-XRT observations. Therefore we conclude that the extended X-ray emission in BAT lightcurves has the same origin as the rapid decay in XRT lightcurves, which has the power-law spectral shape

and also shows rapid spectral softening with time scale of 100 – 1000 sec.

3.2. Exponential Decay in Early Phase

In § 2.5, we adopt both BPL and EXP functions for the lightcurves of rapid decay phase. According to the reduced χ^2 values in Table 2, it is difficult to distinguish which model is more appropriate function to describe the rapid decay phase. This is because, in general, the XRT starts the follow-up observations after ~ 100 sec since GRB triggers and hence the lightcurves are already steeply declining. Moreover small flaring activities disturb the baseline shape of early decay phase.

In BPL model, the best fit temporal index is $-5 \sim -6$ after the break time. In the standard afterglow model, i.e. synchrotron radiation from high-energy electrons accelerated by a relativistic shock, the steepest temporal index is $t^{(2-3p)/4}$ corresponding to the temporal evolution in the highest-energy spectral segment (Piran 1999). Here the parameter p is the power-law index of the energy distribution of accelerated electrons. If we assume the temporal index of -5 and -6 , the corresponding index is $p = 22/3$ and $p = 26/3$, respectively. These are too soft to realize in the usual particle acceleration. Therefore we should include an additional idea to describe the steep decay.

On the other hand, in the EXP model, the observed time constant seems to be much the same as 50 – 100 sec for all events with the rapid decay phase. In the case of long GRBs, the lightcurves of the early X-ray decay phase can be described by the EXP model (O’Brien et al. 2006; Sakamoto et al. 2007; Willingale et al. 2010; Nathanail, Contopoulos, and Basilakos 2014; Imatani et al. 2015). Especially, Imatani et al. (2015) first reported an obvious evidence of the exponential decay from the prompt emission to the following rapid decay (prompt tail) phase of GRB 100418A in 0.7 – 7.0 keV energy band combined with MAXI-SSC and *Swift*-BAT data. Its decay constant of 31.8 ± 1.6 sec is similar to the time scale of SGRBs shown in this paper. Therefore, because of the analogies between long and short GRBs, the EXP model may be appropriate to describe the time behaviour of rapid decay in SGRBs.

Yonetoku et al. (2008) and Moretti et al. (2008) reported similar rapid decline in time with strong spectral evolution in long GRBs. Especially Yonetoku et al. (2008) interpreted the temporal and spectral behavior as dynamic evolution of a spectral model, i.e., a spectral model of a broken power-law with an exponential cut-off moves through the observational energy window of XRT during the rapid decay phase. Here the physical interpretation of the break energy and the cutoff energy is the E_{peak} corresponding to the minimum energy of accelerated electrons and the synchrotron cutoff, respectively. In this paper, we cannot investigate similar and detailed analyses because of limited photon fluxes, but the dynamic spectral evolution may be a possible explanation for the observed temporal and spectral evolution in SGRBs.

We additionally study a possibility that the start time of extended emission is different from the trigger time of short prompt emission. As shown in Figure 1, the peak times of extended emission in BAT lightcurves are about 80 sec and 50 sec for GRB 050724 and GRB 080503, re-

spectively. Therefore we redefine the origin of start time to these peak times, and measure the temporal index of rapid decay phase. When we adopt the BPL model to the time-shifted lightcurves, we obtained the temporal index of $\alpha_1 = 0.32 \pm 0.01$, $\alpha_2 = 3.72 \pm 0.14$, and the break time of $t_b \sim 94$ sec for GRB 050724, and $\alpha_1 = 1.22 \pm 0.07$, $\alpha_2 = 4.03 \pm 0.21$, and $t_b \sim 125$ sec for GRB 080503. We can recognize these temporal indices are still steeper than the general GRB afterglow phenomena, and conclude that the extended emission really shows the rapid decay in time.

3.3. Correlation between temporal and spectral indices

According to the previous sub-sections of § 2.3 and § 2.4, both temporal and spectral indices vary as a function of time. When we describe the energy flux as $F_\nu \propto t^{-\alpha} \nu^{-\beta}$, there is a well-known correlation between α and β as $\alpha = \beta + 2$ ($\beta = \Gamma - 1$), so called α - β correlation, that is realized if a uniform relativistic jet suddenly stops the emission and the high-latitude emission dominates the flux (Kumar & Panaitescu 2000). It is important to understand the emission mechanism and geometry of SGRB's emitting regions. Therefore we systematically investigate the α - β correlation.

To estimate a gradient of the lightcurve, we first adopt the exponential function to describe the rapid decay. After that, we numerically calculate the exponential function and create the pseudo lightcurve with the best fit parameters. Finally, we divide the pseudo lightcurve into the same time intervals as in the spectral analyses, and applied the power-law spectral model to the time resolved pseudo lightcurve. By doing this, we can avoid the disturbance from fluctuations and small flares, and estimate the basic trend of the rapid decay phase. (If we directly estimate the temporal index from lightcurve data, we frequently obtain unrealistic temporal index because of the rattled shape of lightcurves.) Here, we again emphasize that the temporal indices are measured from lightcurves with time resolved spectral analyses in our work, while previous works converted the photon counting rate to the energy flux with averaged spectral parameters.

In Figure 5, we show α - β correlations of GRB 050724, 080503 and 100702A. The error size in the temporal index α is a representative value of $\Delta\alpha = \pm 0.8$ when we directly measure the temporal power-law index by using neighboring three points in the observed lightcurve. The solid line is the expected function of $\alpha = \beta + 2$ for high-latitude emission from a uniform jet (Kumar & Panaitescu 2000). The dashed lines are the best fit function for each SGRB.

The best fit function is $\beta + 2 = (0.5 \pm 0.1)\alpha + (1.6 \pm 0.3)$ for GRB 050724, $\beta + 2 = (0.3 \pm 0.1)\alpha + (1.6 \pm 0.2)$ for GRB 080503, and $\beta + 2 = (0.4 \pm 0.4)\alpha + (2.3 \pm 0.7)$ for GRB 100702A, respectively. In these results, the slopes of the linear fits are similar to each other, and inconsistent with the high-latitude emission of the slope 1 with more than 3σ statistical level. The intercept values of the linear fits are different from each other.

Finally, let us argue possible implications of the observed α - β correlation for the SGRB models. The extended emission is most likely caused by the long-lasting activity of the central engine because the rapid decay is very steep while the external shock emission can not generally produce such large variabilities in the afterglow

lightcurves (Ioka et al. 2005)¹¹. Then the rapid decay phase at $\delta t \sim 100$ sec signals the quenching of the jet from the central engine.

The important point of our finding is that the temporal decay of the extended emission becomes even faster than those produced by the high-latitude emission from quenching uniform jets, as one can see from Figure 5. This means that the contribution from the high-latitude emission is smaller than that of a uniform jet. Therefore the emission geometry of the jet should not be uniform; the brightness declines significantly outside the solid angle of $\theta_{jet} \gtrsim 1/\Gamma \sim 0.01$ on the line-of-sight, where Γ is the bulk Lorentz factor of the jet and is larger than ~ 100 to avoid the compactness problem. Although this may imply the jet opening angle is small or patchy in the extended emission and rapid decay phase (Yamazaki et al. 2004), a typical opening angle of a SGRB jet is usually $\theta \sim 0.1$, much larger than $1/\Gamma$ (Fong et al. 2014; Nagakura et al. 2014; Nakamura et al. 2014; Mizuta & Ioka 2013). A natural solution to this inconsistency may be that the emission comes from a photosphere (Rees & Mészáros 2005; Ioka et al. 2007; Pe'er et al. 2012). The photospheric radius becomes large outside the viewing angle of $1/\Gamma$ for a relativistic jet because the photosphere is concave for $v/c > 2/3$ while it is convex for $v/c < 2/3$ as shown by (Abramowicz et al. 1991). Therefore the high-latitude emission from the photosphere is suppressed even if the jet is uniform.

Additionally, we investigate the α - β correlation for the time shifted lightcurve of GRB 050724 and GRB 080503. We exclude GRB 100702 because it does not show the obvious extended emission in BAT lightcurve and we can not determine its start time as shown in Figure 1. Then we estimated the temporal index of α with the same method as explained above except for the time shift of 80 s and 50 s for GRB 050724 and 080503, respectively.

In Figure 6, we again show the α - β correlation for the time shifted data. The best fit function is $\beta + 2 = (0.5 \pm 0.1)\alpha + (2.3 \pm 0.2)$ for GRB 050724, and $\beta + 2 = (0.3 \pm 0.1)\alpha + (1.8 \pm 0.1)$ for GRB 080503. The slopes of these results are consistent with the previous ones before the time shift, and still inconsistent with the slope of 1 expected from the high-latitude emission. Even if we consider the time shifted lightcurves, at least one data point is still clearly in the region of $\alpha > \beta + 2$ as shown in Figure 6. Therefore the above discussions may be also adopted in this case.

The observed α - β correlation may reflect the angular structure of the photosphere. It is an interesting problem to study whether the α - β correlation is reproduced in the photosphere model or not. Alternatively, the observed α - β correlation may be directly produced by the declining jet emission. In the black hole model with fallback accretion, the Blandford-Znajek process is the most likely mechanism to launch a relativistic jet (Blandford & Znajek 1977), and the rapid decay in X-ray corresponds to the magnetic field decay via reconnection

¹¹ If the density bump of the circumburst medium decelerates the jet down to the Lorentz factor less than the inverse of the opening angle $\Gamma < \theta_j^{-1}$, the light curve might decline steeply, although 1 dimensional simulations are not conclusive (Mimica & Giannios. 2011; Mesler et al. 2012).

at the black hole, which reduces the energy extraction from the rotating black hole (Kisaka & Ioka 2015). Although currently we cannot predict the spectral evolution, our observations should give a clue to the unknown mechanism of the jet emission.

3.4. Population statistics of extended emission

In this paper, we selected the brightest 9 SGRBs in early X-ray flux observed by *Swift*-XRT. The 8 of them are also the brightest events in fluence of BAT observation including the extended emission if it exists, except for 3 SGRBs with the observation start time of ~ 200 s which is later than the usual.¹² These 8 events are satisfied with the criteria of BAT fluence of $> 3.4 \times 10^{-7}$ erg cm $^{-2}$ and XRT flux of $> 10^{-11}$ erg cm $^{-2}$ s $^{-1}$ from selected 92 SGRB candidates. In our sample, only GRB 100702A is the outlier of dimmer fluence in BAT observation but brighter in XRT.

Focusing on these 8 events, the ratio of SGRBs with extended emission is 37.5 %. Bostanci (2013) found 7 % of SGRBs have the extended emission in BATSE data, and Norris, Gehrels & Neil (2010) and Sakamoto et al. (2011) reported 25 % and 2 % in BAT data, respectively. These statistical values should not be directly compared because our and their criteria are different from each other. But, in this paper, we found that the early X-ray flux observed by XRT is strongly affected by the long lasting tail of extended emission. Therefore, our criteria including the early X-ray flux will be important for the future investigation.

3.5. Conclusions

In conclusion, we find the following properties of SGRBs:

1. The spectra of the extended soft X-ray emission and following rapid decay phase can be described by a power-law function with spectral softening. We can exclude a simple thermal blackbody function.
2. The rapid decay phase usually follows the extended X-ray emission.
3. The X-ray lightcurve from the extended emission to the rapid decay phase can be fitted by the exponential function with the time constant of 50 – 100 sec.
4. The high latitude emission can not explain the temporal and spectral behaviour of the extended emission and rapid decay, because the observations do not follow the expected α - β correlation ($\alpha = \beta + 2$).
5. The extended X-ray emission may be observed in 37.5 % of bright SGRBs on the selection criteria of BAT fluence of $> 3.4 \times 10^{-7}$ erg cm $^{-2}$ and XRT flux of $> 10^{-11}$ erg cm $^{-2}$ s $^{-1}$.

ACKNOWLEDGMENTS

This work is supported in part by the Grant-in-Aid from the Ministry of Education, Culture, Sports, Science and Technology (MEXT) of Japan, No. 25103507,

¹² GRB 101219A, 140930B, and 080426 are excluded.

25247038, 15H00780 (DY), No. 24103006, 15H02087 (TN), No. 24340048, 26610048 (KT), No. 26287051, 24103006, 24000004, 26247042 (KI). KK is supported by NASA through Einstein Postdoctoral Fellowship grant number PF4-150123 awarded by the Chandra X-ray Center, which is operated by the Smithsonian Astrophysical Observatory for NASA under contract NAS8-03060.

REFERENCES

- Abramowicz, M. A., Novikov, I. D., & Paczynski, B. 1991, *ApJ*, 369, 175
- Nathanail, A., Contopoulos, I., and Basilakos, S. arXiv:1407.6550
- Cucchiara, A., Prochaska, J. X., Perley, D., et al 2013, *ApJ*, 777, 94
- Barkov, M. V., & Pozanenko, A. S. 2011, *MNRAS*, 417, 2161
- Berger, E. 2014, *ARA&A*, 52, 43
- Berger, E. & Soderberg, A. M. 2005, *GCN Circular*, 4384
- Berger, E. Fong, W., & Chornock, R. 2013, *ApJ*, 774, L23
- Blandford, R. D., & Znajek, R. L. 1977, *MNRAS*, 179, 433
- Bostanci, Z. F., Kaneko, Y., & Gogus, E., 2013, *MNRAS*, 428, 1623
- Bucciantini, N., Metzger, B. D., Thompson, T. A., & Quataert, E. 2012, *MNRAS*, 419, 1537
- Eichler, D., Livio, M., Piran, T. and Schramm, D. N., 1989,
- Fan, Y. Z., Zhang, B., & Proga, D. 2005, *ApJ*, 635, L129
- Fong, W., Berger, E., Metzger, B. D., et al. 2014, *ApJ*, 780, 118
- Gao, W.-H., & Fan, Y.-Z. 2006, *Chinese J. Astron. Astrophysics*, 6, 513
- Gompertz, B. P., O'Brien, P. T., Wynn, G. A., & Rowlinson, A. 2013, *MNRAS*, 431, 1745
- Graham, J. F., Fruchter, A. S., Levan, A. J., et al. 2007, *GCN Circular*, 6836
- Hotkezaka, K., Kyutoku, K., Okawa, H., Shibata, M., & Kiuchi, K. 2011, *Phys. Rev. D*, 83, 124008
- Imatani, R., Tomida, H., Nakahira, S., et al. 2015, *PASJ*, accepted, arXiv:1507.03772
- Ioka, K., Kobayashi, S., & Zhang, B. 2005, *ApJ*, 631, 429
- Ioka, K., Murase, K., Toma, K., Nagataki, S., & Nakamura, T. 2007, *ApJ*, 670, L77
- Kisaka, S., & Ioka, K. 2015, arXiv:1503.06791
- Kisaka, S., Ioka, K., & Takami, H. 2015, *ApJ*, 802, 119
- Kumar, P. & Panaitescu, A. 2000, *ApJ*, 541, L51
- Kyutoku, K., Ioka, K., & Shibata, M. 2013, *Phys. Rev. D*, 88, 041503
- Kyutoku, K., Ioka, K., Okawa, H., Shibata, M., & Taniguchi, K. 2015, arXiv:1502.05402
- Lee, W. H., Ramirez-Ruiz, E., & López-Cámara, D. 2009, *ApJ*, 699, L93
- Mesler, R. A., Whalen, D. J., Lloyd-Ronning, N. M. et al & 2012 *ApJ*, 757, 117
- Metzger, B. D., Quataert, E., & Thompson, T. A. 2008, *MNRAS*, 385, 1455
- Mimica, P. & Giannios, D. 2011, *MNRAS*, 418, 583
- Mizuta, A., & Ioka, K. 2013, *ApJ*, 777, 162
- Moretti, A., Margutti, R., Pasotti, F., et al. 2008, *A & A*, 478, 2, pp.409-417
- Nakamura, T., Kashiyama, K., Nakauchi, D., et al. 2014, *ApJ*, 796, 13
- Nagakura, H., Hotokezaka, K., Sekiguchi, Y., Shibata, M., & Ioka, K. 2014, *ApJ*, 784, L28
- Norris, J. P., Gehrels, & Neil, Scargle, J. D., 2010, *ApJ*, 717, 411
- O'Brien, P. T., Willingale, R., Osborne, J., et al. 2006, *A & A*, 647, 1213
- Paczynski, B., 1986, *ApJ*, 308, L43
- Pe'er, A., Zhang, B. B., Ryde, F., McGlynn, S., Zhang, B., Preece, R. D., Kouveliotou, C. 2012, *MNRAS*, 420, 468
- Piran, T. 1999, *Physics Report*, 314, 575
- Prochaska, J. X., Bloom, J. S., Chen, H-W. et al. 2005, *GCN Circular*, 3700

- Rau, A., McBreen S., Kruehler, T., & Greiner, J. 2009, GCN Circular, 9353
- Rees, M. J., & Mészáros, P. 2005, ApJ, 628, 847
- Rosswog, S. 2007, MNRAS, 376, L48
- Sakamoto, T., Hill, J. E., Yamazaki, R., et al., 2007, ApJ, 669, 1115
- Sakamoto, T., Barthelmy, S. D., Baumgartner, W. H., et al., 2011, ApJS, 195, 27
- Tanvir, N. R., Levan, A. J., Fruchter, A. S. et al. 2013, Nature, 500, 7464, 547–549
- Takami, H., Nozawa, T., & Ioka, K. 2014, ApJ, 789, L6
- Usov, V. V. 1992, Nature, 357, 472
- Willingale, R., Genet, F., Granot, J., et al. 2010, MNRAS, 403, 1296
- Yamazaki, R., Ioka, K., & Nakamura, T. 2004, ApJ, 607, L103
- Yonetoku, D., S. Tanabe, T. Murakami, et al. 2008, PASJ, 60, SP1, pp.S352–S360
- Zhang, B., & Mészáros, P. 2001, ApJ, 552, L35
- Zhang, B. 2013, ApJ, 763, L22

TABLE 1
SAMPLES OF SHORT GRB

ID	redshift	$T_{90,obs}$ (sec)	χ^2 (d.o.f) of E.E.	reference
GRB 050724	0.258 ^a	98.7	105.3 (23)	^a Prochaska et al. (2005)
GRB 051221A	0.5465 ^b	1.4	17.9 (23)	^b Berger & Soderberg (2005)
GRB 060313	—	0.8	21.9 (23)	
GRB 070714B	0.92 ^c	65.2	59.9 (23)	^c Graham et al. (2007)
GRB 080503	—	274.9	712.8 (23)	
GRB 090510	0.903 ^d	0.4	23.2 (23)	^d Rau et al. (2009)
GRB 100702A	—	0.2	18.3 (23)	
GRB 120804A	—	1.8	23.2 (23)	
GRB 130603B	0.3586 ^e	0.18	14.5 (23)	^e Cucchiara et al. (2013)

TABLE 2
TEMPORAL PROPERTIES OF EARLY X-RAY EMISSION (EXTENDED EMISSION OR AFTERGLOW) OF SGRBs

ID	model	index α_1	break time t_b	index α_2	time const. τ	χ^2	d.o.f
GRB 050724	PL	2.63 ± 0.19	—	—	—	280	19
	BPL	2.03 ± 0.07	187	5.90 ± 0.53	—	55.2	17
	EXP	—	—	—	52.2 ± 0.9	81.7	19
GRB 051221A	PL	0.77 ± 0.04	—	—	—	4.0	2
	BPL	0.66 ± 0.03	25700	1.47 ± 0.24	—	0.3	0
	EXP	—	—	—	192 ± 39	103	2
GRB 060313	PL	1.11 ± 0.04	—	—	—	5.5	4
	BPL	1.07 ± 0.03	20100	2.07 ± 0.37	—	4.9	2
	EXP	—	—	—	305 ± 60	93.7	4
GRB 070714B	PL	2.33 ± 0.06	—	—	—	76.2	6
	BPL	1.58 ± 0.17	117	2.64 ± 0.14	—	67.7	4
	EXP	—	—	—	68.3 ± 4.0	100	6
GRB 080503	PL	3.34 ± 0.22	—	—	—	143	11
	BPL	2.27 ± 0.12	179	5.06 ± 0.29	—	24.4	9
	EXP	—	—	—	51.9 ± 1.3	18.3	11
GRB 090510	PL	1.17 ± 0.03	—	—	—	19.0	6
	BPL	0.93 ± 0.01	10200	1.97 ± 0.35	—	4.7	4
	EXP	—	—	—	706 ± 87	39.1	6
GRB 100702A	PL	1.72 ± 0.16	—	—	—	13.2	2
	BPL	0.74 ± 0.05	192	6.13 ± 0.30	—	0.002	0
	EXP	—	—	—	91.1 ± 8.6	8.0	2
GRB 120804A	PL	0.93 ± 0.04	—	—	—	8.9	2
	BPL	0.78 ± 0.03	14800	1.91 ± 0.24	—	5.3	0
	EXP	—	—	—	1260 ± 140	46.2	2
GRB 130603B	PL	0.83 ± 0.05	—	—	—	4.72	2
	BPL	0.75 ± 0.02	8880	1.89 ± 0.33	—	1.57	0
	EXP	—	—	—	2130 ± 300	31.7	2

TABLE 3
STATUS OF EARLY X-RAY PROPERTY OF SGRBs

ID	extended emission	rapid decay	spectral evolution
GRB 050724	YES	YES	YES
GRB 051221A	NO	NO	NO
GRB 060313	NO	NO	YES
GRB 070714B	YES	NO	YES
GRB 080503	YES	YES	YES
GRB 090510	NO	NO	NO
GRB 100702A	NO ^a	YES	YES
GRB 120804A	NO	NO	NO
GRB 130603B	NO	NO	NO

^a The flux level of extended emission may be under the sensitivity of BAT

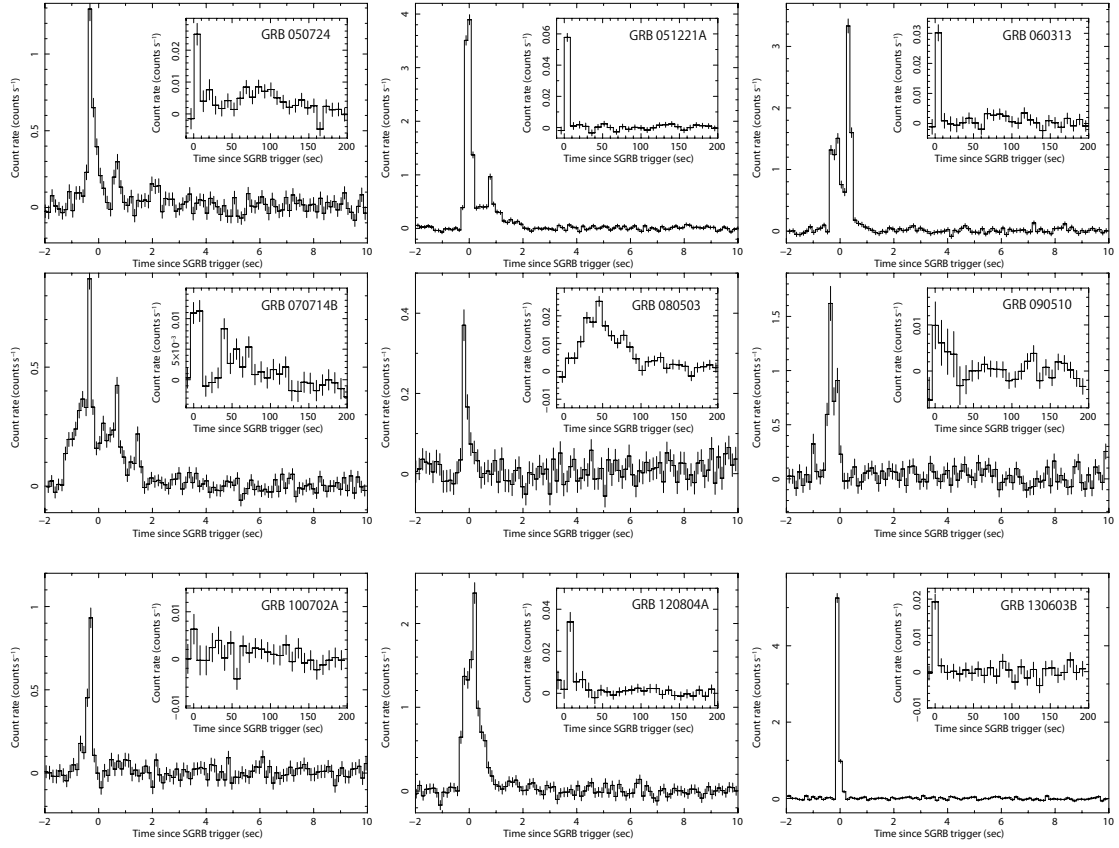


FIG. 1.— *Swift*-BAT lightcurves of bright 9 SGRBs. The main panels show lightcurves of prompt emission with 128 msec time resolution in 15–150 keV band. The inserted panels also show the following long-lasting X-ray emission up to 200 sec since SGRB trigger with 8 sec time resolution in 15–25 keV band. We can clearly confirm extended X-ray emission for 3 events (GRB 050724, 070714B and 080503).

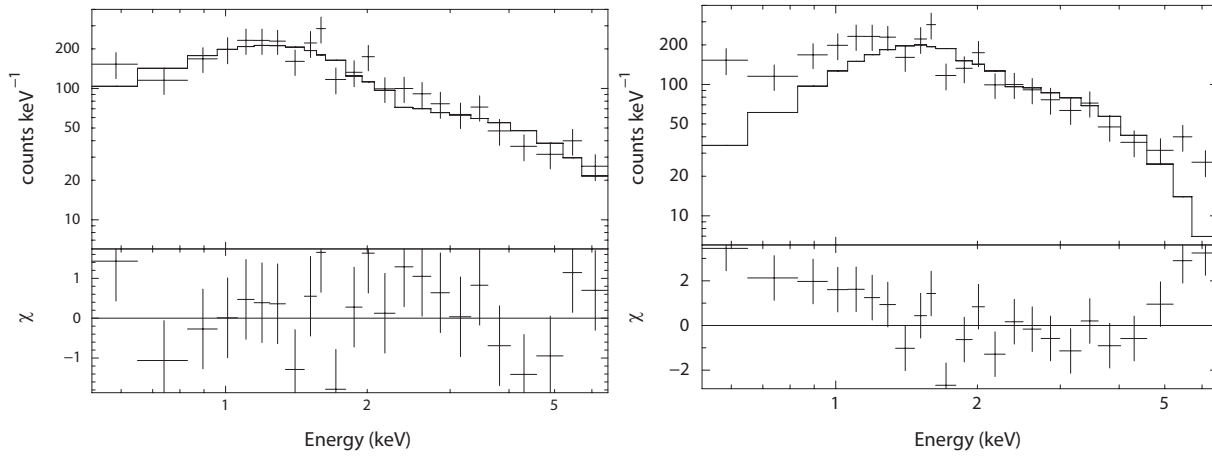


FIG. 2.— Examples of spectral fittings of XRT data. Top and bottom panels are the observed spectra (including detector response) and the fitting residuals of the best fit functions. (Left) Fitting result of GRB 080503 with the absorbed power-law model (Equation 1). (Right) Same as the left but with the blackbody function (Equation 2).

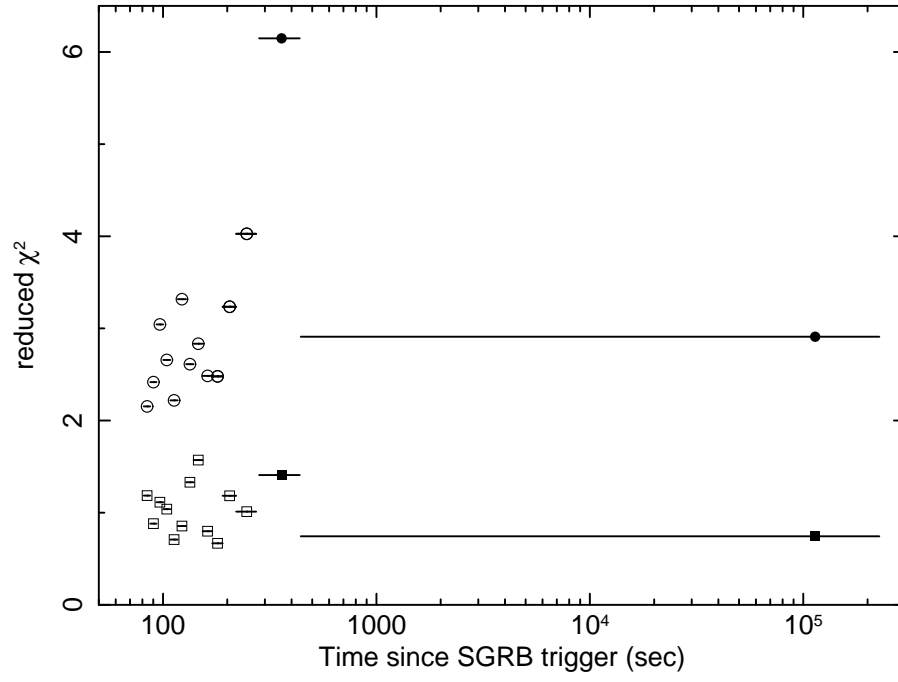


FIG. 3.— Reduced χ^2 distributions of the best fit spectral model of power-law (square) and blackbody (circle) for time resolved spectra of GRB 080503. The open and filled squares are the result of the power-law model for WT and PC mode data, respectively. The open and filled circles are the same but for the blackbody model, respectively.

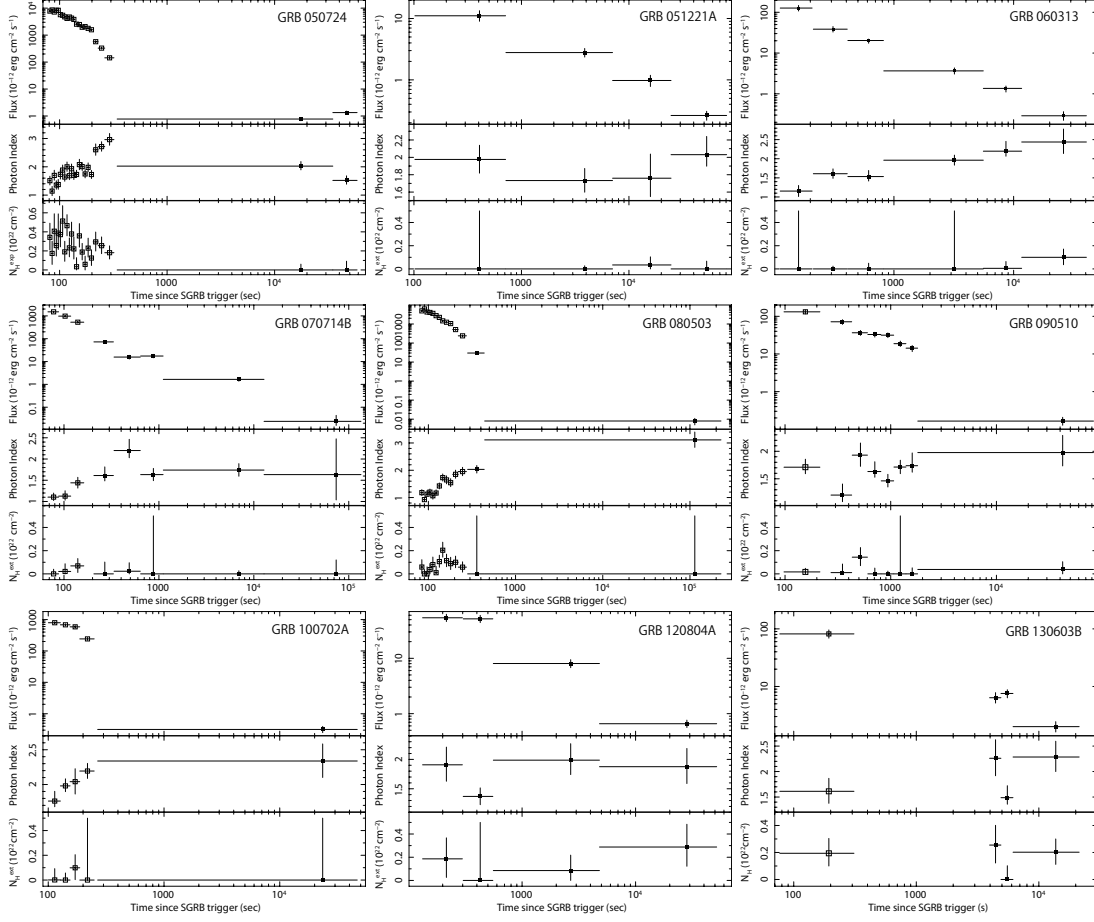


FIG. 4.— (Top panel) Observed X-ray lightcurves by *Swift*-XRT. Open and filled squares indicate the data of WT mode and PC mode of *Swift*-XRT observations, respectively. Each energy flux in 2.0–10.0 keV is measured by time resolved spectral analyses. (Middle panel) The photon indices obtained by spectral fittings with the absorbed power-law model (Equation 1). (Bottom panel) The extra-galactic column density N_{H}^{ext} in units of 10^{22} cm^{-2} .

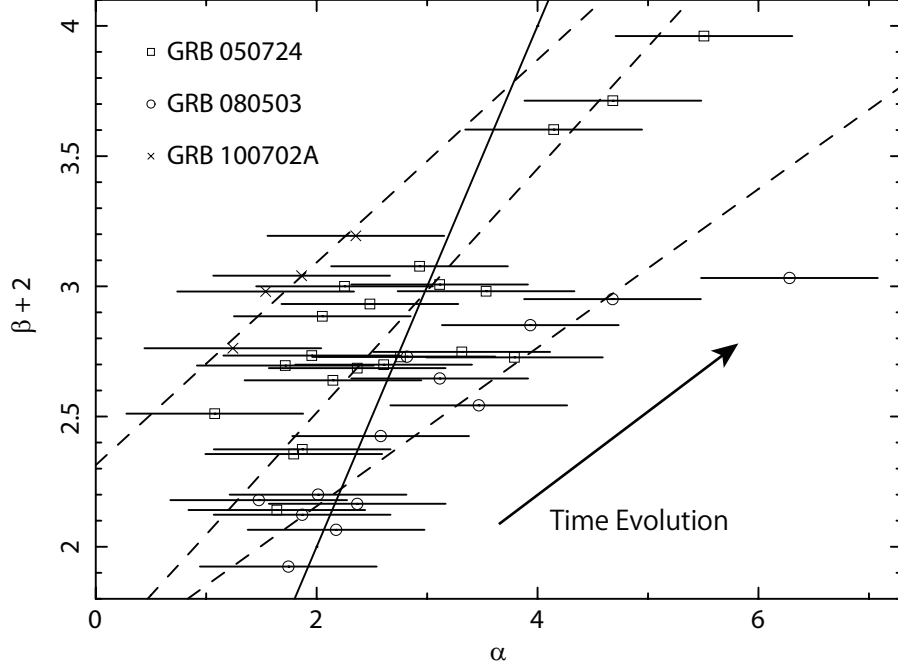


FIG. 5.— Correlations between temporal and spectral indices of three SGRBs, GRB 050724 (open squares), 080503 (open circles) and 100702A (crosses). The solid line is the expected function of $\alpha = \beta + 2$ for the high-latitude emission of spherically symmetric shells, and the dashed lines are the best fit linear function for each event. For GRB 050724 and GRB 080503, both correlations cross the solid line at $t \sim 110$ sec and $t \sim 152$ sec since the SGRB trigger time, respectively.

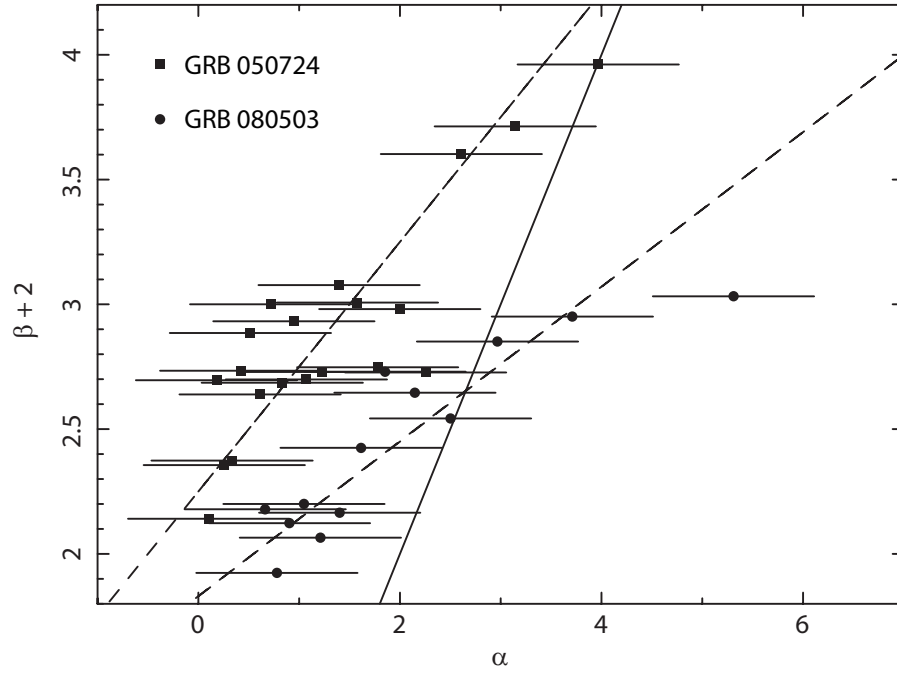


FIG. 6.— Correlations between temporal and spectral indices of GRB 050724 (filled squares) and 080503 (filled circles) after shifting the time origin by 80 s and 50 s, respectively. The meanings of solid and dashed lines are the same as Figure 5.